CHAPTER 4

ANTIFOULING BEHAVIOUR OF PVDF/TiO_2 COMPOSITE MEMBRANE: A QUANTITATIVE AND QUALITATIVE ASSESSMENT

This chapter deals with the antifouling behavior PVDF/TiO_2 composite membranes prepared via the phase inversion technique. Different amounts of TiO_2 with respect to the weight of the polymer were incorporated in the casting solution to study qualitatively and quantitatively the antifouling property of the membrane. The membrane morphology was studied using a high-resolution scanning electron microscope (HRSEM) and atomic force microscope (AFM).The interfacial interactions between foulants and TiO_2 immobilized membranes were also evaluated using the extended Derjaguin–Landau–Verwey–Overbeek (XDLVO) approach. The XDLVO theory revealed an increase in repulsive interactive energy barrier with increase in TiO_2 loading. Thus it improves the antifouling property of the membrane. Intercalation of TiO_2 nanoparticles efficiently improved the porosity and wettability of the polymeric membranes was confirmed from the contact angle analysis. The modified PVDF membranes exhibited excellent antimicrobial properties against Gram-negative *E.coli (Escherichia coli)* bacteria as confirmed by the halo zone and activity tests. The permeation experiment results showed high rejection of Bovine Serum Albumin (BSA) and humic acid (HA) (foulants) for PVDF membranes with optimum TiO_2 loading (PM3- 2 wt%). However, it was also observed that at 3 wt% TiO_2 (PM4) membranes exhibited a negative effect on these characteristics due to non-uniform distribution of TiO_2.

4.1 INTRODUCTION

Membrane separation technology is widely used for getting potable and industrial grade water for various applications (Salimi and Yousefi 2003, Elimelech and Phillip, 2011). Fouling of membrane affects the hydraulic permeability requiring frequent replacement of the fouled membrane thereby increasing the overall cost of the process (Wang et al., 2014, Lin et al., 2015). Therefore the membrane fouling has been a subject of interest of researchers since long (Le-Clech et al., 2006). The bio-fouling of the membrane is initiated by the adhesion, growth, and multiplication of one or more bacterial species onto the membrane surface, which eventually leads to the formation of a cake layer on the membrane surface (Hong et al., 2013). In recent studies, it has been concluded that the prime factor affecting membrane fouling is its interfacial property (Buonomenna et al., 2007) which controls membrane-foulant interactions hence the adsorption of foulant on the membrane surface (Chang et al., 2015). Hydrophilicity and hydrophobicity are the prime factors affecting fouling, and it has been recognized that hydrophilic membranes are less prone to fouling compared to hydrophobic membranes (Weis et al., 2005). Based on this information, strategies like graft polymerization, chemical grafting, and surface coating have been considered to improve the surface hydrophilicity and modify membrane characteristics (Salimi and Yousefi, 2003). The main disadvantages of these approaches include weak interaction between polymer and additives (blending) affect the long term durability or instability of coated layer (surface modification) causes a release from the membrane (Salimi and Yousefi, 2003).

Among various methods used, incorporation of inorganic particles into the polymer matrix to form a composite membrane is an effective approach to enhance membrane

hydrophilicity and antifouling property (Mo et al., 2007). Different inorganic nanomaterials such as TiO_2 (Li et al., 2013), SiO_2 (Yang et al., 2006), Al_2O_3 (Yan et al., 2009), graphene oxides (Wang et al., 2012), and carbon nanotubes (Brunet et al., 2008) have been widely used to fabricate composite membranes. However, nano-sized TiO_2, due to its superior hydrophilicity, antibacterial property, and chemical stability has received much attention (Diebold et al., 2003). Addition of TiO_2 nanoparticles improves antifouling property due to change in hydrophilicity, porosity, zeta potential, and surface roughness (Wang et al., 2014).

Further, preparation of anti-biofouling membranes by coupling antimicrobial materials with polymeric matrix has also attracted the attention of many researchers in both academia and industry. There are two interesting approaches to kill bacteria before colonization- i) release killing and ii) contact killing (Zhang et al., 2016). Leaching of antibacterial agents on the membrane surface is termed as release killing, but there is continuous depletion of biomaterial that may cause environmental risk and significantly reduce antibacterial efficiency. As a result, the need for developing composite membranes with the contact-killing surface and stable and long-term anti-biofouling activities has attracted the attention of researchers (Zhang et al., 2016). Inorganic metal oxides are being preferred over organic antimicrobial agents due to their stability, robustness, and long shelf-life (Raghupathi et al., 2011). Titanium dioxide (TiO_2) is the widely used nanomaterial because of its stability, hydrophilicity, nontoxic, and anti-fouling properties (Subramaniam et al., 2017, Almeida et al., 2016)

Most of the available published works have reported the experimental methods to characterize the antifouling property of the membrane. A systematic investigation of the

interaction of nanoparticles in improving the antifouling property is has not been attempted. In this work the efficacy of these membranes has been investigated by using extended Derjaguin-Landau-Verwey Overbeek (XDLVO) theory, for the first time. The experimental results are compared with theoretical predictions for evaluating the antifouling property of membranes and effect of adding nanoparticles on this property. Effect of loading of TiO_2 nanoparticles on the antifouling property of PVDF membrane prepared by the phase-inversion membranes is evaluated by measuring the pure water flux and rejection efficiency of bovine serum albumin (BSA) and humic acid (HA) along with the study of the bactericidal behaviour and underlying the anti-microbial effects are studied using Gram-negative bacteria *(Escherichia coli).*

4.1.2 The XDLVO Theory

The extended Derjaguin–Landau–Verwey–Overbeek (XDLVO) theory explains the exact role of hydrophilicity/ hydrophobicity and effects of all other physiochemical factors on the membrane surface energetics (interfacial interaction between membranes and foulants (Zhang et al., 2015). The theory assumes that the attachment of foulant with membrane surface is due to three type of interactions caused by- i) Lifshitz–van der Waals (LW) forces, ii) polar or Lewis acid-base (AB) interactions, and iii) electrostatic (EL) interactions (Lin et al., 2014)

The XDLVO theory considers the attachments of foulant to the membrane surface by evaluating the contribution of surface interactions (Wang et al., 2016). According to Oss (1995), the total free energy of adhesion is the result of contribution of these three parameters and is expressed as

$$U_{mbc}^{XDLVO} = U_{mbc}^{LW} + U_{mbc}^{EL} + U_{mbc}^{AB} \quad (4.1)$$

where U_{mlc}^{XDLVO} is the total interfacial free energy between the membrane and the foulant, U_{mbc}^{LW}, U_{mbc}^{EL}, and U_{mbc}^{AB} represent individual components of the total interfacial energy, whereas m, b, c represent membrane, bulk liquid (water) and foulant (BSA), respectively. The individual energy is calculated using equations 4.2, 4.3, and 4.4 given below.

$$U_{mbc}^{LW} = 2\pi \Delta G_{ho}^{LW} h_o^2 \frac{a}{h} \quad (4.2)$$

$$U_{mbc}^{AB} = 2\pi a \lambda \Delta G_{ho}^{AB} \exp\frac{(ho-h)}{h} \quad (4.3)$$

$$U_{mbc}^{EL} = \pi\varepsilon a\{2\zeta_c\zeta_m \ln\left(\frac{1+e^{-kh}}{1-e^{-kh}}\right) + (\zeta_c^2 + \zeta_m^2)\ln(1-e^{-2kh})\} \quad (4.4)$$

where a is the radius of foulant (BSA), h is the separation distance between the membrane and the foulant, h_o is the minimum separation distance (0.158nm), λ is the decay length (value taken as 0.6 nm for aqueous solution) (Safarpour et al., 2014), ζ_c, and ζ_m are the zeta potential of the foulant and the membrane, k is the inverse Debye screening length. The values of ΔG_{ho}^{LW} and ΔG_{ho}^{AB} were calculated using equations 4.5 and 4.6, respectively:

$$\Delta G_{ho}^{LW} = 2\left(\sqrt[2]{\gamma_b^{LW}} - \sqrt[2]{\gamma_m^{LW}}\right)\left(\sqrt[2]{\gamma_f^{LW}} - \sqrt[2]{\gamma_b^{LW}}\right) \quad (4.5)$$

$$\Delta G_{ho}^{AB} = 2\sqrt[2]{\gamma_b^+}\left(\sqrt[2]{\gamma_m^-} - \sqrt[2]{\gamma_c^-} - \sqrt[2]{\gamma_b^-}\right) + 2\sqrt[2]{\gamma_b^-}\left(\sqrt[2]{\gamma_m^+} - \sqrt[2]{\gamma_c^+} - \sqrt[2]{\gamma_b^+}\right) - 2\left(\sqrt[2]{\gamma_m^+\gamma_c^-} + \sqrt[2]{\gamma_m^-\gamma_c^+}\right) \quad (4.6)$$

where γ^{LW},γ^{+}, γ^{-} are LW component, electron acceptor and donor parameter, respectively. The surface tension of membrane ($\gamma_m^{LW}, \gamma_{m,}^{-}, \gamma_m^{+}$) and BSA were quantified using extended Young's equation. This equation shows the relationship between the contact angle of a liquid and the surface tension parameter of both liquid and solid surface and is evaluated using equation 4.7

$$(1+\cos\theta)\gamma_l^{TOT} = 2\left(\sqrt[2]{\gamma_s^{LW}}\gamma_l^{LW} + \sqrt[2]{\gamma_s^{+}}\gamma_l^{-} + \sqrt[2]{\gamma_s^{-}}\gamma_l^{+}\right) \quad (4.7)$$

where θ is the contact angle and γ_l^{TOT} is the sum of LW and AB and is calculated using equation 4.8

$$\gamma_l^{TOT} = \gamma^{LW} + \gamma^{AB} \quad (4.8)$$

The polar component γ^{AB} of the material is expressed by equation 4.9

$$\gamma^{AB} = 2\,(\gamma^{+}\gamma^{-})^{0.5} \quad (4.9)$$

Above equations have been used to calculate relevant parameters for comparison with experimental values as discussed ahead.

4.2 EXPERIMENTAL PROCEDURE

4.2.1 Materials

Polyvinylidene fluoride (PVDF), n-methyl-2-pyrrolidone (NMP), and TiO_2 nanoparticles (Degussa P25 (25nm), a hydrophilic metal oxide) were purchased from Sigma-Aldrich (Bombay, India). Diiodomethane, glycerol, nutrient broth (NB) as media and nutrient agar (NA) were obtained from High Media (Bombay), bovine serum albumin (BSA), humic acid (HA) was obtained from SD Fine Chemicals Ltd. (Bombay, India) and

phosphate buffer saline (PBS) were obtained from Merck. Double distilled water (DD) used in all experiments was prepared in the laboratory.

4.2.2 Synthesis of TiO_2 NPs and PVDF/TiO_2 Composite Membranes

The particle and membrane were synthesized as already described in Chapter 3 Sections 3.2.2 a and 3.2.2.b

4.2.3 Physiochemical Properties of Membranes

4.2.3.a Contact Angle Measurement

The wetting characteristic of membranes was evaluated by measuring the contact angle of the composite membrane surface with a contact angle goniometer [KRUSS, DSA 4, Germany] using the sessile drop method. 3 µl droplet of distilled water was used as the probe liquid at the ambient temperature.

4.2.3.b Morphological Characterization

The membrane surface was examined using a high- resolution scanning electron microscope (Nova Nano SEM 450, USA). The membrane films were initially coated by sputtering with gold, and the photomicrographs were taken under very high vacuum. The Scanning Probe Microscope (NTEGRA Prima, NT-MDT Service & Logistic Ltd., USA) was used to detect the surface roughness of the synthesized membranes under the non-contact mode.

4.2.3.c Antibacterial Characteristics

4.2.3.c.a Halo Zone Test

The antibacterial efficacy of PVDF/TiO_2 membranes was evaluated using the Halo Zone method. Prior to the tests, all the materials used were autoclaved at 120 ℃ for 1 h to ensure sterility. Cultivation of *E. coli* was carried out for 24 hours in a conical flask containing the sterilized solution of NB (1.3g NB/100 ml water) placed in an incubator maintained at 37°C. During this period, the bacteria were fully grown, and then 100µl of the bacterial suspension was spread over the agar plate composed of 1.3g of NB and 2.3g of NA in 100 ml distilled water. The UV treated membrane pieces of approximately 1cm diameter were now placed on the agar plates and again incubated at 37°C for 24 h. The extent of inhibition zone formation around the membrane pieces indicated the antibacterial behaviour of the membranes (Du et al., 2015).

4.2.3.c.b Bacterial Growth

All glass-wares, the nutrient broth solution, and all other solutions were autoclaved at 120°C for 60 min. The membrane pieces of known area (1 cm x 1 cm) were first rinsed three times with 0.01 M fresh sterile phosphate buffered saline (PBS, pH 7.4) followed by sterilization through UV irradiation for half an hour. A bacterial suspension (10^{-3} cells/100ml) was prepared in the sterile nutrient broth. The UV treated membrane pieces were then immersed in the above suspension. Subsequently, the flasks containing pieces of different composite membranes and bacterial suspensions were incubated in a rotary shaker at 100-105 rpm at 37°C in the absence of any light. The growth of *E. coli* was measured in terms of optical density at 600 nm (OD_{600}) (Kim and Lee 2016) at several incubation times

(t = 0, 6, 12, 18, and 24 h) using a spectrophotometer (SYSTRONICS, PC Based Double Beam Spectrometer 2202, Bombay, India). Each reported value was obtained by averaging 10 individual measurements. Data of the exponential growth phases were fitted using the pseudo-first-order kinetics:

$$\ln(x_t/x_o) = \mu t \quad (4.10)$$

$$\tau_d = \ln 2/\mu \quad (4.11)$$

where x_o and x_t represent values of OD_{600} for the bacterial suspensions at 0 and t h, respectively, μ is the specific growth rate (h^{-1}), and τ_d represents the doubling time (h). The adhesion and growth of *E.coli* on membrane surface was observed using, HRSEM (High resolution scanning electron microscope)

4.2.4 Water Permeation Studies

The pure and composite PVDF membranes with the filtration area of 15.5 cm^2 were used in a flow filtration cell to test the fouling behaviour using BSA as the model foulant (1 g/L, pH7.5). Initially, the synthesized membranes were compacted at 0.2 MPa to achieve a stable flux, and then a pure water flux $Q_w(kg/m^2h)$ was measured at 0.1 MPa for 1.5 h then it was replaced by the BSA solution. Permeation of BSA was recorded as Q_F and concentrations of feed and permeates were evaluated using UV spectrophotometer by measuring the absorbance at 280 nm (Oh et al., 2009).

$$Q_w = M/(Axt) \quad (4.12)$$

where M is the permeate mass (kg), A is the membrane area (m^2), and t is the permeation time (h). The rejection percentage (R) of BSA was calculated from equation 4.13

$$R= (1- B_p/B_f) x100 \quad (4.13)$$

B_p and B_f (mg/ml) are the concentrations of BSA in permeate and feed, respectively. The fouled membranes were rinsed with water, and the water permeability was again measured as Q_{WR}. The regeneration test was carried out to analyze the recovery and self-cleaning ability of membranes which was calculated using equation 4.14.

$$FRR = Q_{WR} /Q_w x100 \quad (4.14)$$

where Q_{WR} is the water flux after each cycle (kg/m^2 h) and Q_w is the initial pure water flux (kg/m^2 h), FRR represent flux recovery ratio. The filtration experiment with 5 mg/L HA at 0.2 MPa for 1.5 h was conducted to further evaluate the antifouling property of composite membrane, following the same procedure as described above by replacing BSA solution with HA solution. The water flux before and after contact with HA solution was measured, and flux decline was calculated in terms of relative fluxes.

4.3 RESULTS AND DISCUSSION

4.3.1 Physiochemical Properties of the Membrane

4.3.1.1Atomic Force Microscopy (AFM) Analysis

The AFM photomicrographs given in Figure 4.1 show the effect of TiO_2 loading on the membrane surface roughness. In a 3D AFM image, the bright portion represents the highest peak on the membrane surface whereas the dark portion represents valleys. It is a well-

known fact that smoother the membrane surfaces the lesser will be the fouling tendency (Meng et al., 2016). In case of membranes with a rough surface accumulation of foulants will occur within the "valleys" and such membranes will foul easily. Figure 4.1depicts that membrane PM1 (no TiO_2), exhibits several large peaks and valleys, i.e., it has a very rough surface. The decrease in roughness parameter indirectly enhances the antifouling property of the polymeric membrane. AFM images clearly depicts disappearance of large valleys with increasing TiO_2 loading thus tendency of membrane pore filling with foulants is reduced. This analysis elucidates that smoothness is more influential in controlling the membrane fouling by restricting the interaction between foulant and membrane surface/pores than membrane hydrophilicity. Also hydrophilicity was investigated using contact angle (Chapter 3, section 3.3.4) which did not provide a precise quantitative measurement, as it still lacks in explaining the relative changes of a membrane property by fouling. Roughness is defined in terms of three parameters- i) mean roughness (R_a) defined as average deviation of the z-values, which is half the average peak to valley depth, ii) root mean square roughness (R_q) which represents standard deviation of an entire z-values, and iii) average of height (R_z) expressed as the difference of largest positive and negative z-values (Wang et al., 2014).

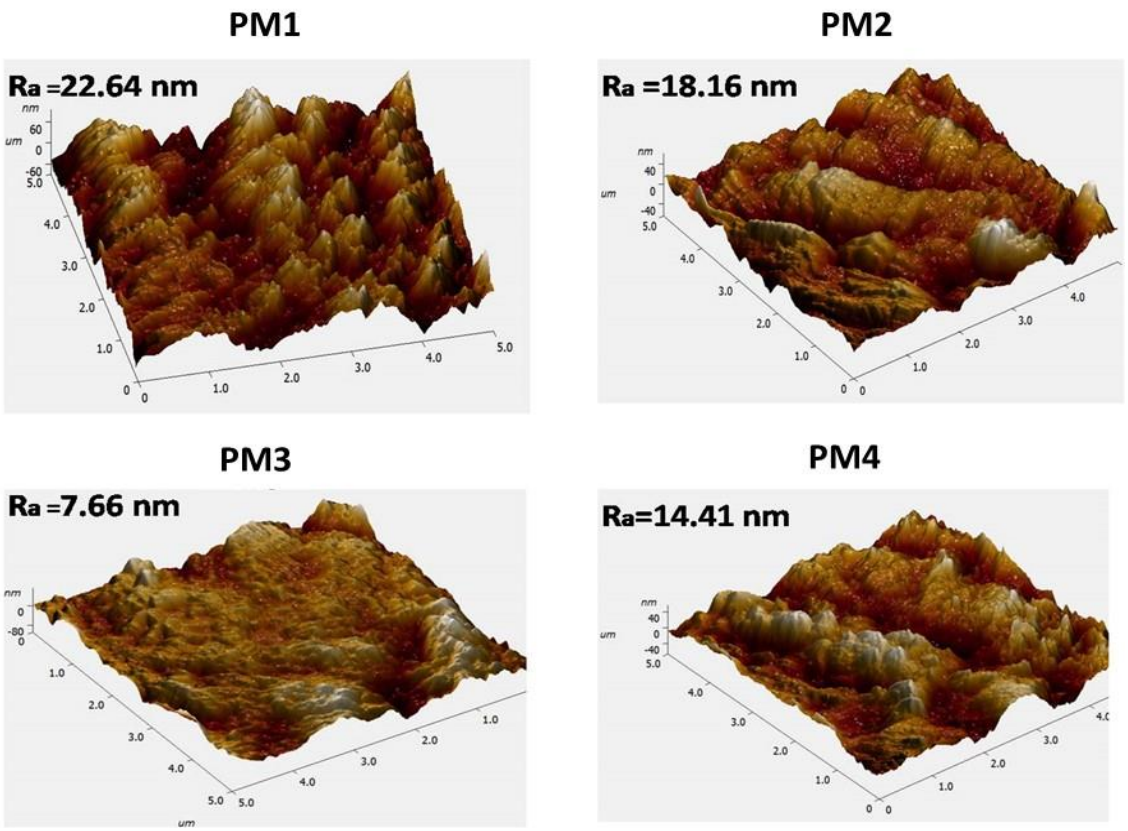

Figure 4.1: 3-D AFM image of different PVDF composite membranes.

The values of these roughness parameters for different composite membranes are listed in Table 4.1, (AFM scanning area of 5 μm x 5 μm). The results indicate that surface roughness decreases with increase in the concentration of TiO_2, but the membrane M4 with the highest loading exhibits higher roughness; this is likely to be due to the presence of aggregated particles (Zhao et al., 2013). Excessive addition of TiO_2 particles in the matrix results in bumps formation hence increases the peak value. Similar results are also reported in the literature (Zinadini et al., 2014).

Table 4.1: Roughness parameter of PVDF and its composite membrane

Sample	R_a (nm)	R_q(nm)	R_z (nm)
PM1	22.64	22.76	74.45
PM2	18.16	23.68	61.94
PM3	07.66	09.78	29.88
PM4	14.41	17.03	43.88

4.3.2 XDLVO Theory based Analysis of Fouling Behaviour

A better understanding of the fouling mechanism of the membranes can be obtained by estimating the physicochemical interactions between the foulant and composite membrane. The surface tension parameters of membranes were calculated using the Young-Dupré equation by using the measured contact angles of 3 different probe liquids with known parameters (Tables 4.2, 4.3 and 4.4). The results show that the value of electron donor component (γ^-) is always greater than that for the electron acceptor component (γ^+) indicating that all the membranes exhibit high electron donor mono-polarity that varies from 1.522 to 2.804 mJ m^{-2}. The results are consistent with the reported values (He et al., 2018). It was also found that membrane PM4 is having the highest values of (γ^+) and (γ^{AB}) compared to other membranes indicating high polar properties.

The high values of electron donor components (γ^-) for TiO_2 modified PVDF membranes indicate mono-polar hydrophilic surface due to the presence of hydrophilic TiO_2 nanoparticles.

Table 4.2: **Contact angle value of 3 different probe liquids**

Contact Angle	Ultrapure water	Diiodometane	Glycerol
PM1	86.7	62.8	70.1
PM2	78.2	57.9	63.8
PM3	72.6	53.6	59.2
PM4	74.8	55.1	61.7

Table 4.3: **Surface tension values (mJ m^{-2}) of 3 probe liquids**

Probe liquid	γ^{LW}	γ^{+}	γ^{-}	γ^{AB}	γ^{TOT}
Ultrapure water	22.1	25.5	25.5	50.7	72.8
Diiodometane	50.8	0	0	0	50.8
Glycerol	34	3.92	57.4	30	64

The increase in γ^{TOT} with increasing TiO_2 loading in membranes means strong interfacial molecular affinity between the membrane and water molecules. A tightly bound formation of the steric-entropic barrier will restrain the interaction between the membrane surface and foulant hence delays the fouling (Rincon and Pulgarin 2003).

The individual surface free energy AB and LW parameters were calculated using equations (4.5) and (4.6). The sum of these two energy components for any given material gives the free energy of cohesion (ΔG^{TOT}). It provides a quantitative perception regarding the hydrophilicity and hydrophobicity. The thermodynamic theory suggests that adhesion or attraction between two materials occurs when ΔG^{TOT} is negative. Higher the negative value stronger is the hydrophobicity, intense is the attraction between membrane and foulant, hence more severe will be the membrane fouling.

Table 4.4: The surface tension and surface free energy of membranes

Sample	γ^{LW}	γ^{+}	γ^{-}	γ^{AB}	γ^{TOT}	ΔG_{ho}^{LW}	ΔG_{ho}^{AB}	ΔG^{TOT}
PM1	5.199	1.268	1.522	3.859	9.058	-10.548	-50.718	-61.267
PM2	5.464	1.280	2.328	5.959	11.423	-10.298	-42.906	-53.204
PM3	5.685	1.280	2.804	7.178	12.863	-10.094	-38.328	-48.422
PM4	5.609	1.649	2.231	7.358	12.967	-10.163	-41.963	-52.126

It is also observed that ΔG^{TOT} is more negative for pure PVDF membrane, indicating it to be more hydrophobic and hence a stronger attraction between the membrane and the foulant(Rincon and Pulgarin 2003).The value increases on increasing the TiO_2 loading, and is significant for membrane PM3, indicating a less force of attraction between the foulant (BSA) and the membrane. Further increase in TiO_2 loading increases the agglomeration of the particles, resulting in a reduction in the free energy of cohesion for PVDF/TiO_2 membranes. These values were further used to calculate the individual interaction energy parameters based on which total interaction energy U_{mlc}^{XDLVO} was evaluated. The plots of interaction energy as a function of separation distance are shown in Figure 4.2. The figure exhibits the effect of interaction energy on membrane fouling. It is seen that as the separation distance increases the interaction energy gradually approaches zero. The figure also predicts that the foulant needs to overcome the repulsive force to get attached to the membrane surface. The higher the repulsive barrier, the harder it will be for the foulant to get attached (Wang et al., 2014). For the membranes used in this work the energy barrier follows the order PM3>PM4>PM2>PM1. As a result deposition or blocking of membrane surface for M3 is minimal. Thus it is seen that improving the membrane hydrophilicity by adding TiO_2 will diminish the membrane fouling.

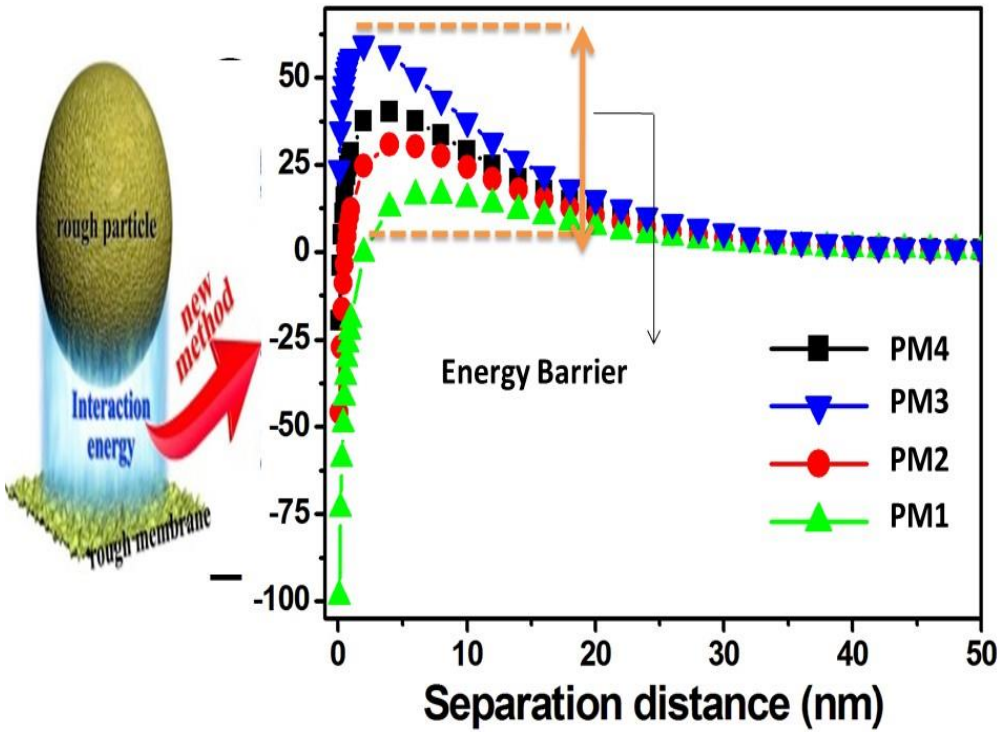

Figure 4.2: Variation of interaction energy between membrane and BSA

These results provide a quantitative picture of the interfacial interactions between foulants and membrane based on XDLVO theory. From the contact angle values and the results of XDLVO theory, it can be said that fouling of membrane can be mitigated by strengthening the interface polarity and hydrophilicity

4.3.3Antibacterial Property

4.3.3.a Halo Zone Test

The Halo zone tests were used to qualitatively investigate the antibacterial property of pure PVDF and TiO_2 incorporated membranes against gram-negative bacteria (*E.coli*) after 24 h of incubation at 37 °C. Figure 4.3 shows the strength of the inhibition zone, an area around the membrane piece without any growth of bacteria after 24 h. These figures depict

that the pristine PVDF (PM1) being hydrophobic does not exhibit inhibition zone hence has no antibacterial activity. All membranes with TiO_2 exhibit inhibition zone formation, but the zones for PM3 and PM4 membranes are more prominent. Thus it can be said that the inherent antibacterial property of TiO_2 protects the membrane from fouling by not allowing bacteria to grow in the nearby region.

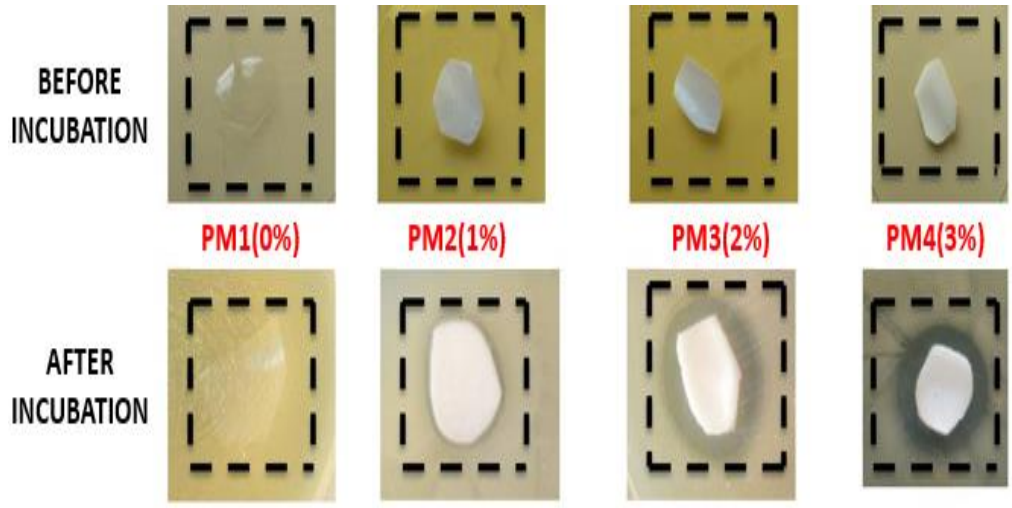

Figure 4.3: Inhibition zone formation for different PVDF composites membrane

4.3.3.b Bacterial Growth

The Gram-negative (*E.coli*) bacteria were used to test the antimicrobial activity of pristine PVDF and PVDF/TiO_2 membranes. The OD_{600} values during and after 24 h incubation are shown in Figure 4.4. These figures indicate that membranes PM3 and PM4 exhibit significant inhibition capacity towards *E. coli* strains.

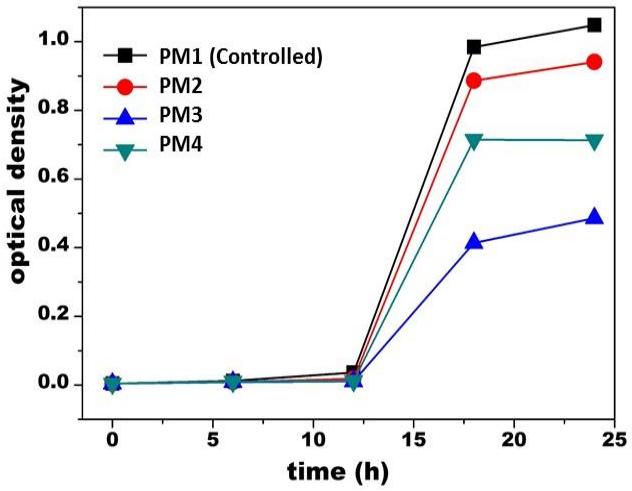

Figure 4.4: The OD_{600} plot for PM1(control, no TiO_2), PM2, PM3, and PM4 incubated for 24h.

The viability of bacteria on the pure and composite membrane surface before and after incubation for 24 h was determined by HRSEM. Figure 4.5 depicts the adhesion and growth of *E. coli* on the pure PVDF and composite membranes. It is clear that the surface of membrane PM1 is covered with a large number of bacteria while that of membrane PM3 with the least number. It can be attributed to the disruption of the cell wall due to the presence of nanoparticles (Caballero et al., 2009). These results are consistent with the results of AFM and contact angle values since membrane PM1 having a high value of roughness and being hydrophobic is more susceptible to fouling compared to the membrane PM3with the lowest roughness value as shown in AFM result in Figure 4.1 and the hydrophilic characteristics. The HRSEM images exhibiting the growth behaviour of bacteria are shown in Figure 4.5 and it is observed that the trend for the growth of bacteria over the membrane surface is similar to that observed for the biocidal activities obtained from OD_{600} measurements.

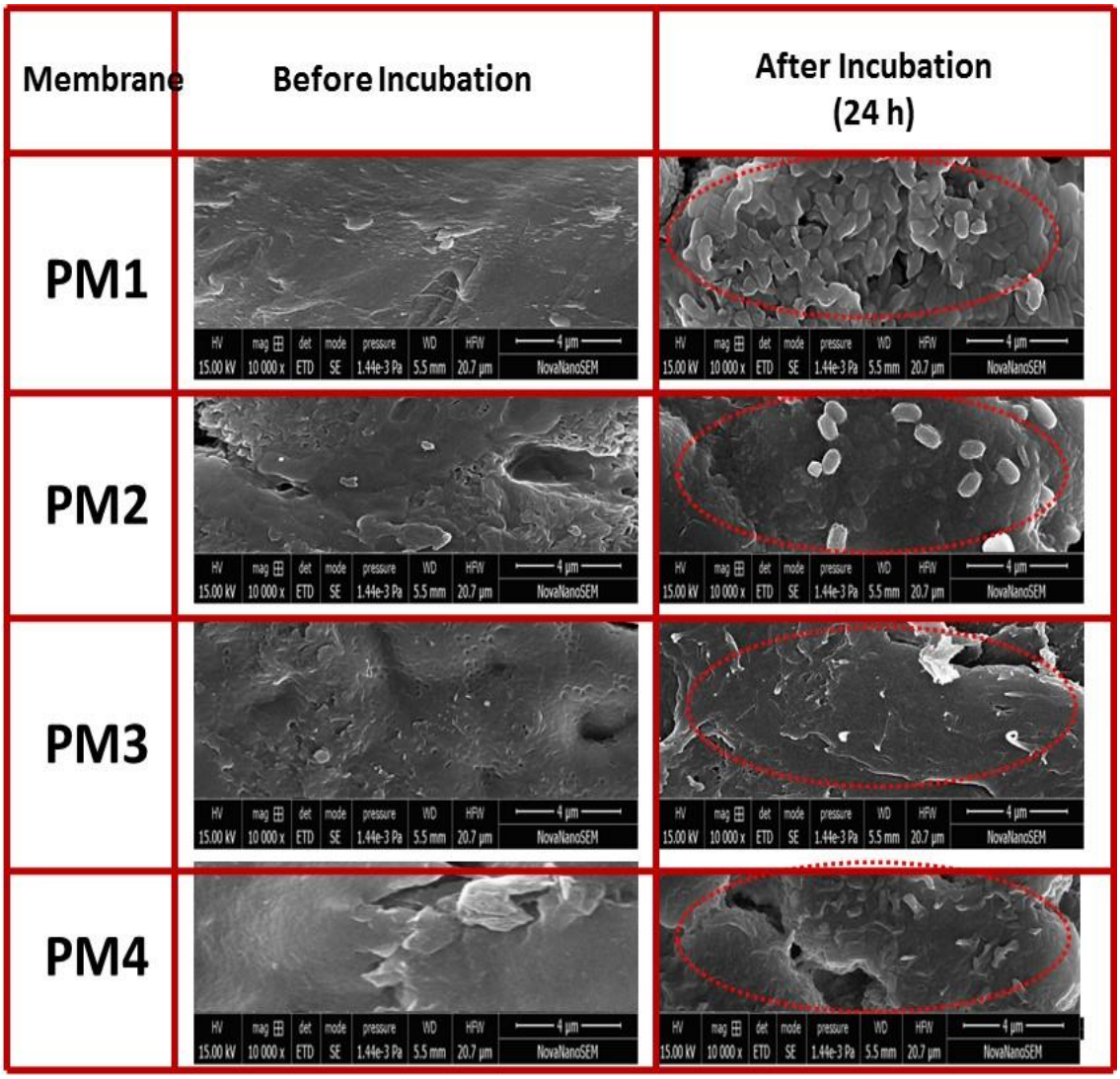

Figure 4.5: HRSEM images of PVDF-TiO_2membranes before and after bacterial growth.

The cell proliferation of *E.coli* was studied for the exponential growth phase for 3–24 h to see the inhibition by nanocomposite membrane. The results reveal that specific growth rate (μ) of *E. coli* is very high in the presence of pristine PVDF but decreases dramatically with increase in TiO_2 loading. The increase in the doubling time τ_d (Figure 4.6) was also observed. The optimal growth inhibition is not observed for the highest TiO_2

loading (PM4 membrane), due to agglomeration of particle leading to the availability of less active sites for *E.coli* cells to get killed.

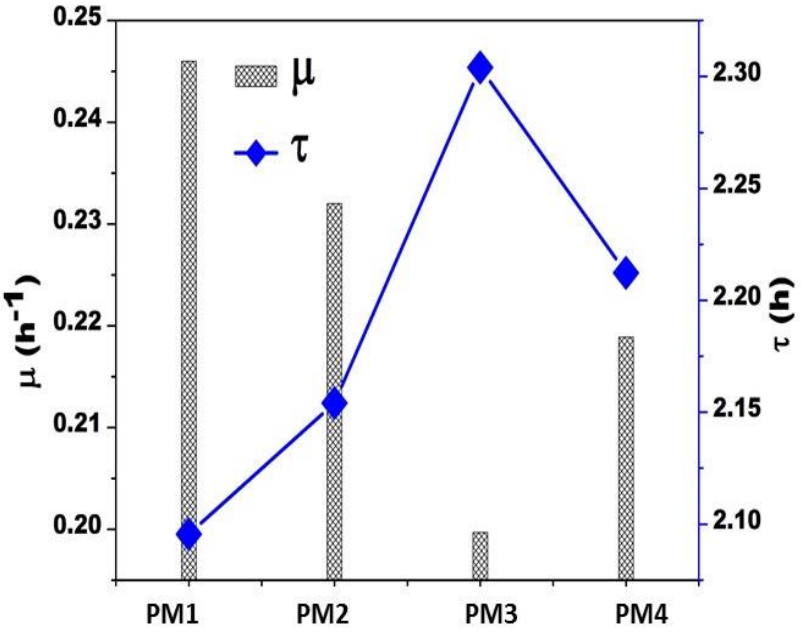

Figure 4.6: Antibacterial activity of different composite membranes

At low concentrations, TiO_2 does not cover the entire membrane surface as a result; some bacteria grow. The membrane PM3 results in intimate contact between TiO_2 particles and the bacteria affecting the bacterial cell wall and in turn leading to enhancement in the antibacterial effect (Rahimpour et al., 2011). Anti-bacterial activity is reduced for membrane PM4. At higher concentrations, due to particles agglomeration, the surface is not completely covered with TiO_2 nanoparticles leaving space for the bacteria to grow (Dutta et al., 2015). The present results confirm that TiO_2 exhibits anti-bactericidal activity, and the results consistent with those of Rahimpour et al. (2011). Further, aggregation of TiO_2 NPs results in the loss of available surface area causing reduction in anti-fouling ability.

4.3.4 Permeate Flux

4.3.4.a Performance against BSA

A qualitative evaluation of the antifouling property of membranes was carried out by measuring the water flux using BSA as the model foulant. The water flux values before and after BSA filtration are shown in Figure 4.7a. An improvement in flux with an increase in TiO_2 loading from 0 to 3 wt% is observed. This enhancement is due to the hydrophilic nature of TiO_2. For membrane PM4, flux has declined due to agglomeration of TiO_2 particles (Dutta et al., 2015). Through the second cycle of runs it is observed that the decline in the pure water flux is the highest for pristine PVDF membrane compared to composite membranes. The same trend was observed in the third and fourth cycle with a small change in FRR suggesting the stability performance of the nanocomposite membrane. These results are in agreement with the results obtained from the XDLVO theory, where the energy barrier follows the order PM3>PM4>PM2>PM1.This confirmed that the deposition or blocking of membrane surface for PM3 is minimal. The flux recovery ratio (FRR) of composite membranes is shown in Figure 4.7b. The graph represents the increase in values of FRR for modified membrane indicating better reuse, antifouling and cleaning property of the composite membrane.

The rejection% for various membranes is shown in Figure 4.7c. This trend is expected because a higher flux recovery ratio means less fouling of the membrane surface. Increase in nanoparticle loading reduces the roughness hence the foulant will not be able to accumulate on to membrane surface rather it will be rejected easily resulting in a high flux.

4.3.4.b Performance against HA

To further, examine the antifouling property of nanocomposite membranes ultrafiltration experiments with HA solution were conducted. The variation of relative flux with time is shown in Figure 4.7 d. The figure depicts a decrease in the fouling tendency of PVDF/TiO_2 membrane compared to pure PVDF. A maximum resistance against fouling was observed for PM3 membrane having the lowest contact angle and least roughness as shown in Table 4.2 and Figure 4.1, respectively. The probability of adsorption decreases on the membrane surface with the addition of TiO_2 nanoparticles is a consequence of increasing membrane hydrophilicity. Adsorption of foulant is considered as the first step causing membrane fouling, and it is dependent on the physicochemical properties of both the membranes and foulants (Xin et al., 2014). It is a well-known fact that hydrophobic surfaces have a higher tendency of fouling, as a result, adsorption occurs relatively quickly for hydrophobic than hydrophilic surfaces (Arsuaga et al., 2010). The addition of TiO_2 nanoparticles decreased the roughness, hydrophobicity which further mitigated the fouling. Thus it becomes significantly important to fabricate membrane with less roughness and improved hydrophilicity to enhance the performance as well as antifouling ability. Hence the results of BSA and HA filtration concludes that TiO_2 incorporated PVDF membranes possess better antifouling characteristic compared to the pristine PVDF with the best result obtained for PM3 membrane in both the cases.

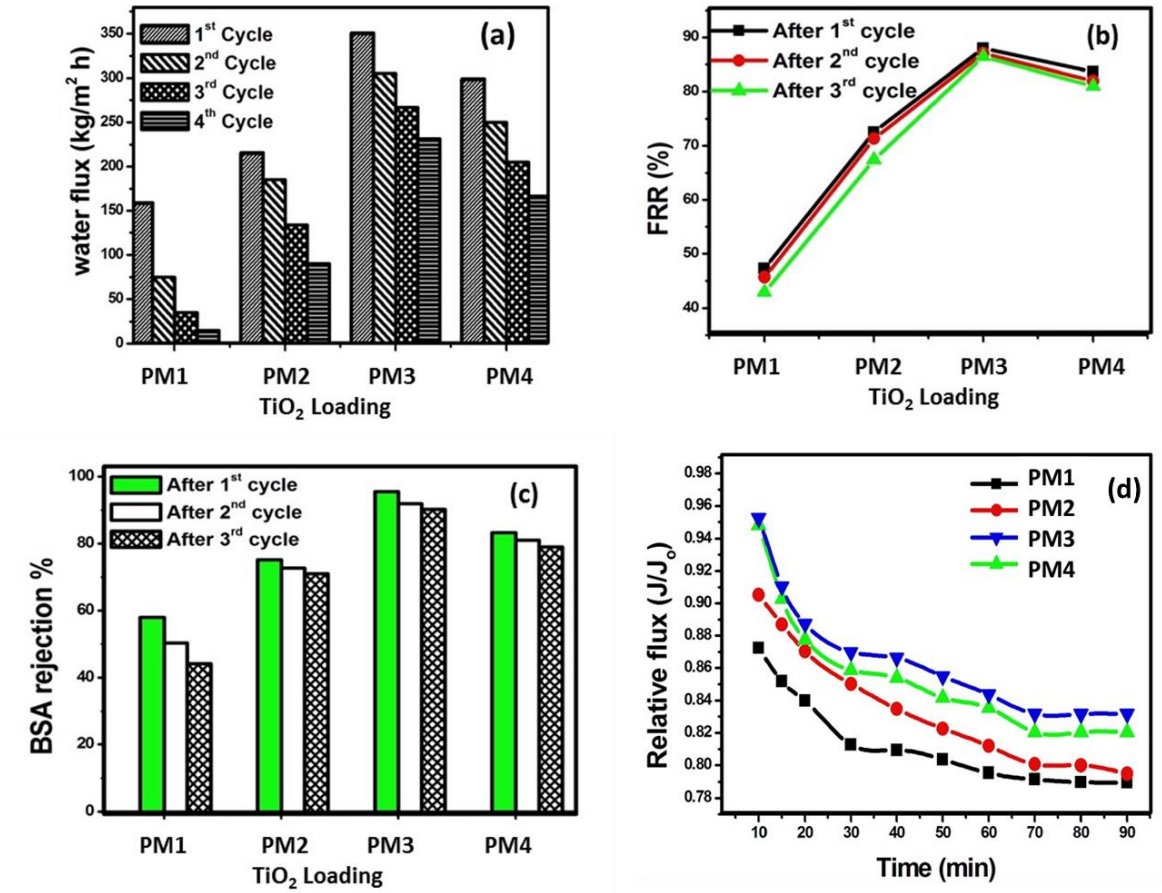

Figure 4.7: (a) Water flux value for different composite membranes before and after filtration of BSA bearing water (b) FRR and (c) % BSA rejection for different PVDF/TiO_2 composite membrane (d) Flux ratio during filtration of HA solution.

Hence it can now be concluded that TiO_2 immobilized PVDF membranes exhibit good rejection and show the potential for water flux recovery A comparison of the relative percentage of, water flux, flux recovery ratio and contact angle for inorganic nanomaterial-PVDF hybrid membranes available in the open literature and PVDF/TiO_2 membranes developed in this work is presented in Table 4.5. It is seen that PVDF/TiO_2 membrane has better characteristics compared to other PVDF composite membranes. Further, compared to other membranes reported in literature the cost of PVDF/TiO_2 membranes can be lower due

to no use of other additives such as (PVP or PES) and low cost of TiO_2 compared to GO NPs indicating their better performance during treatment of wastewater.

Table 4.5: Comparison of the performance of inorganic-polymer nanocomposite membranes prepared in this work and those reported in the literature

Polymer	Solvent	Additive (wt%)	NPs (wt%)	Result	Ref.
PVDF	NMP	Thermoexfoliated Vermiculite Blended poly(ether sulfone) (PES) (5- 20 wt%)	-	**CA*** Approx 85 to 52° **Flux** 330 to 476.4 (L/m^2h) **FRR** 83.77% after 3 cycle	Orooji et al., 2017
PVDF	DMAc (Dimethyl-acetamide)	PVP (0.01) (Polyvinyl-pyrrolidone)	Carbon nanotube (1 wt%) and Graphite oxide (1 wt%)	**CA** Approx 65 and 70° **Flux** 115 and 160 (L/m^2h) **FRR** 72.8% and 85.1%	Zhang et al., 2013
PVDF	DMAc	PVP (0.01)	Graphite oxide (0, 0.5, 1 and 2 wt%)	**CA** Approx 71 to 60° **Flux** 78 to 361.24 (L/m^2h)	Xu et al., 2014
PVDF	DMAc	PVP (0.01)	Graphite oxide (0, 0.5, 1 and 2 g L^{-1})	**CA** 81 to 58° **Flux** 280 to 467.8 (L/m^2h) **FRR-** 42% to 85.7%	Wu et al., 2014
PES	DMF (*N*,*N*-dimethyl-formamide)	-	TiO_2 (0.45 wt%)	**Cleaning efficiency** 17 to 71% (approx)	Li et al., 2016

				FRR 82%	
PVDF	DMAc	PVP	Ag-TiO_2-APTES (0 to 0.5g)	**CA** 81.8 to 61.4° **Rejection %** (MB*) 43.7 to 94.4	Peng et al., 2017
PVDF	DMAc	PVP	TiO_2 (0 to 5 wt%)	**Flux** 155 to 266 (L/m^2h) **Rejection %** (BSA)-85 to 95	Cao et al., 2006
PVDF	NMP	-	TiO_2 (0 to 3wt%)	**CA** 85.4 to 70.2° **Flux** 158 to 350 (Kg/m^2h) **FRR**- 57% to 95%	This work

*CA= Contact Angle, MB= Methylene Blue

4.4 CONCLUSIONS

The incorporation of TiO_2 has enhanced the hydrophilicity, reduced the surface roughness and improved the repulsive interaction energy barrier between the foulant and the membrane, thus resulting in a better antifouling ability of the membrane surface. At higher loadings, aggregation of TiO_2 particles has resulted in increased surface roughness due to the formation of bumps leading to the reduction in the repulsive interaction and decrease in the antifouling characteristics. The composite membrane with optimal TiO_2 loading (PM3- 2 wt%) has shown an excellent flux recovery ratio (approx 95%) compared to other membranes when subjected to 4 cycles of use thus indicating that a membrane with the optimum TiO_2 loading can withstand fouling without affecting the flux. This membrane

has exhibited the highest antifouling ability. Higher TiO_2 loading has resulted in a reduction in active surface sites available for the killing of bacteria.

4.5 REFERENCES

Almeida NA , Martins PM , Teixeira S , Lopes da Silva JA , SencadasVKu¨hn K , Cuniberti G , Mendez SL , Marques PAAP TiO_2/graphene oxide immobilized in P(VDF-TrFE) electrospun membranes with enhanced visible-light induced photocatalytic performance. Journal of Material Science 51(2016)6974–6986

Arsuaga JM, Lopez-Munoz MJ, Sotto A Correlation between retention and adsorption of phenolic compounds in nanofiltration membranes. Desalination 250(2010) 829–832.

Brunet P , Lyon DY , Zodrow K , Rouch JC , Caussat B , Serp P Remigy JC , Wiesner MR , Alvarez PJJ, Properties of Membranes Containing Semi-dispersed Carbon Nanotubes. Environmental Engineering Science 25(2008) 565–575.

Buonomenna MG, Macchi P, Davoli M, Drioli E, Poly(vinylidene fluoride) membranes by phase inversion: the role the casting and coagulation conditions play in their morphology, crystalline structure and properties. European Polymer Journal 43(2007) 1557-1572

Caballero L, Whitehead, KA, Allen, NS, Verran, J, Inactivation of Escherichia coli on immobilized TiO_2 using fluorescent light. Journal of Photochemistry and Photobiology A 202(2009)92–98.

Cao X, Ma J, Shi X, Ren Z, Effect of TiO_2 nanoparticle size on the performance of PVDF membrane. Applied Surface and Science 253(2006) 2003-2010

Chang H , Qu F , Liu B , Yu H , Li K , Shao S , Gi GL , Liang H, Hydraulic irreversibility of ultrafiltration membrane fouling by humic acid: effects of membrane properties and backwash water composition. Journal of Membrane Science 493(2015)723–733.

Damodar RA, Youa S, Chou H, Study the self-cleaning, antibacterial and photocatalytic properties of TiO_2 entrapped PVDF membranes. Journal of Hazardous Material 172(2009)1321–1328

Diebold U, The surface science of titanium dioxide. Surface Science Reports 48(2003)53–229.

Du JR , Peldszus S , Huck PM , Feng X Modification of membrane surfaces via micro swelling for fouling control in drinking water treatment. Journal of Membrane Science 475(2015) 488–495.

Dutta AK, Egusa M, Kaminaka H, Izawa H, Morimoto M, Saimoto H, Ifuku S Facile preparation of surface N-halamine chitin nanofiber to endow antibacterial and antifungal activities. Carbohydrate Polymer 115(2015)342-347.

ElimelechM , Phillip AW The future of seawater desalination: Energy, Technology, and the Environment. Science 333(2011) 712–717.

He Y ,Chen X , Dai F , Xu R , Yang N , Feng X , Zhao Y , Chen L, Immobilization of poly(N-acryoylmorpholine) via hydrogen-bonded interactions for improved separation and antifouling properties of poly (vinylidene fluoride) membranes. Reactive and Functional Polymer 123 (2018)80–90.

Hong H , Peng W , Zhang M , Chen J , He Y , Wang F , Weng X , Yu H , Lin H Thermodynamic analysis of membrane fouling in a submerged membrane bioreactor and its implications. Bioresource Technology 146(2013)7–14.

Kim BS, Lee J Macroporous PVDF/TiO_2 membranes with three-dimensionally interconnected pore structures produced by directional melt crystallization. Chemical Engineering Journal 301(2016) 158–165.

Le-ClechP, Chen V, Fane TAG, Fouling in membrane bioreactors used in wastewater treatment. Journal of Membrane Science 284(2006) 17–53.

Li WY , Sun XL , Wen C , Lu H , Wang ZW Preparation and characterization of poly (vinylidene fluoride)/TiO_2 hybrid membranes. Frontiers of Environmental Science and Engineering 7(2013)492–502.

Li X, Li J, Fang X, Bakzhan K, Wang L, Bruggen BV A synergetic analysis method for antifouling behavior investigation on PES ultrafiltration membrane with self-assembled TiO_2 nanoparticles. Journal of Colloid and Interface Science 469(2016)164–176.

Lin T, Lu Z , Chen W Interaction mechanisms of humic acid combined with calcium ions on membrane fouling at different conditions in an ultrafiltration system. Desalination 357(2015) 26–35.

Lin T , Lu ZJ , Chen W Interaction mechanisms and predictions on membrane fouling in an ultrafiltration system, using the XDLVO approach. Journal of Membrane Science 461(2014) 49–58

Liu X, Chen Q , Lv L , Feng X , Meng X, Preparation of transparent PVA/TiO_2 nanocomposite films with enhanced visible-light photocatalytic activity. Catalysis Communication 58(2015)30–33.

Martins PM , Miranda R , Marques J , Tavares CJ , Botelho G , Lanceros-Mendez S Comparative efficiency of TiO_2 nanoparticles in suspension vs. immobilization into P(VDF–TrFE) porous membranes. RSC Advance 6(2016) 12708–12716.

Meng N , Priestley RCE , Zhang Y , Wang H , Zhang X, The effect of reduction degree of GO nanosheets on microstructure and performance of PVDF/GO hybrid membranes. Journal of Membrane Science 501(2016) 169–178.

Mo J, Son SH, Jegal J, Kim J, Lee YH, Preparation and characterization of polyamide nanofiltration composite membranes with TiO_2 layers chemically connected to the membrane surface. Journal of Applied Polymer Science 105(2007) 1267–1274

Oh SJ. Kim N, Lee YT, Preparation and characterization of PVDF/TiO_2 organic–inorganic composite membranes for fouling resistance improvement. Journal of Membrane Science 345(2009) 13–20.

Orooji Y, Liang F, Razmjou A, Li S, MofidR, Liu Q, Guan K, LiuZ, Jin W, Excellent Biofouling Alleviation of Thermoexfoliated Vermiculite Blended Poly(ether sulfone) Ultrafiltration Membrane. ACS Applied Material Interfaces 9 (35) (2017) 30024–30034.

Peng Y, Yu Z,Pan Y, Zeng G Antibacterial photocatalytic self-cleaning poly(vinylidene fluoride) membrane for dye wastewater treatment. Polymer Advance Technology 29(2017)254–262.

Raghupathi KR, Koodali RT , Manna AC Size-Dependent Bacterial Growth Inhibition and Mechanism of Antibacterial Activity of Zinc Oxide Nanoparticles. Langmuir 27(2011) 4020–4028

Rahimpour A, Jahanshahi M , Rajaeian B , Rahimnejad M TiO_2 entrapped nano-composite PVDF/SPES membranes, Preparation, characterization, antifouling and antibacterial properties. Desalination 278(2011)343–353.

Rincon AG and Pulgarin C, Photocatalytical inactivation of E. coli, effect of (continuous intermittent) light intensity and of (suspended–fixed) TiO_2concentration. Applied Catalysis B 44(2003)263–284.

Safarpour M, Khataee A, Vatanpour V Preparation of a Novel Polyvinylidene Fluoride (PVDF) Ultrafiltration Membrane Modified with Reduced Graphene Oxide/Titanium

Dioxide (TiO_2) Nanocomposite with Enhanced Hydrophilicity and Antifouling Properties. Industrial and Engineering Chemistry Research 53(2014)13370−13382.

Salimi A and Yousefi AA, Analysis Method: FTIR studies of *β*-phase crystal formation in stretched PVDF films. Polymer Testing 22(2003) 699-704.

Subramaniam MN , Goh PS , Lau WJ , Tan YH , Ng BC , Ismail AF, Hydrophilic hollow fiber PVDF ultrafiltration membrane incorporated with titanate nanotubes for decolourization of aerobically-treated palm oil mill effluent. Chemical Engineering Journal 316(2017)101–110.

Van Oss CJ, Hydrophobicity of biosurfaces – origin, quantitative determination and interaction energies. Colloids and Surfaces B: Biointerfaces 5 (3–4) (1995) 91–110.

Wang Q , Wang Z , Zhang J , Wang J , Wu Z Antifouling behaviours of PVDF/nano-TiO_2 composite membranes revealed by surface energetics and quartz crystal microbalance monitoring, RSC Adv 4(2014) 43590-43598.

Wang X , Zhou M , Meng X , Wang L , Huang, D Effect of protein on PVDF ultrafiltration membrane fouling behavior under different pH conditions, interface adhesion force and XDLVO theory analysis. Frontiers of Environmental Science and Engineering 10(4), (2016) 12.

Wang ZH , Yu HR , Xia JF , Zhang FF , Li F , Xia YZ , Li YH Novel GO-blended PVDF ultrafiltration membranes. Desalination 299(2012)50–54.

Weis A, Bird MR, Nyström M, Wright C, The influence of morphology, hydrophobicity and charge upon the long-term performance of ultrafiltration membranes fouled with spent sulphite liquor. Desalination 175 (1)(2005)73–85.

Wu T, Zhou B, Zhu T, Shi J, Xu Z, Hua C, Wang J, Facile and low-cost approach towards a PVDF ultrafiltration membrane with enhanced hydrophilicity and antifouling performance via graphene oxide/water-bath coagulation. RSC Adv. 5(2015)7880-7889

Xin Li, Fang X, Pang R, Li J, Sun X, Shen J, Han W, Wang L Self-assembly of TiO_2 nanoparticles around the pores of PES ultrafiltration membrane for mitigating organic fouling. Journal of Membrane Science 467(2014) 226–235.

Xu Z , Zhang J, Shan M, Li Y , Li B , Niu J , Zhou B , Qian X Organosilane-functionalized graphene oxide for enhanced antifouling and mechanical properties of polyvinylidene fluoride ultrafiltration membranes. Journal of Membrane Science 458(2014) 1–13.

Yan L , Hong S , Li ML , Li YS Application of the Al_2O_3–PVDF nanocomposite tubular ultrafiltration (UF) membrane for oily wastewater treatment and its antifouling research. Separation and Purification Technology 66(2009) 347–352.

Yang YN, Wang P Preparation and characterizations of new PS/TiO2 hybrid membranes by sol–gel process. Polymer 47(2006) 683-2688

Zhang J, Xu Z, Mai W, Min C, Zhou B, Shan M, Li Y, Yang C,Wanga Z, Qiana X Improved hydrophilicity, permeability, antifouling and mechanical performance of PVDF composite ultrafiltration membranes tailored by oxidized low dimensional carbon nanomaterials. Journal of Material Chemistry A 1(2013) 3101

Zhang M , Liao B , Zhou X , He Y , Hong H , Lin H , Chen J Effects of hydrophilicity/hydrophobicity of membrane on membrane fouling in a submerged membrane bioreactor. Bioresource Technology 175(2015) 59–67.

Zhang X , Wang Z , Chen M , Liu M , Wu Z, Polyvinylidene fluoride membrane blended with quaternary ammonium compound for enhancing anti-biofouling properties, Effects of dosage. Journal of Membrane Science 520(2016) 66–75.

Zhao C , Xu X , Chen J , Yang F Effect of graphene oxide concentration on the morphologies and antifouling properties of PVDF ultrafiltration membranes. Journal of Environmental Chemical Engineering 1(2013) 349–354.

Zinadini S, Zinatizadeh AA, Rahimi M, Vatanpour V, Zangeneh H, Preparation of a novel antifouling mixed matrix PES membrane by embedding graphene oxide nanoplates. Journal of Membrane Science 453(2014) 292–301

CHAPTER 5

SYNTHESIS OF PVDF/TiO_2 MEMBRANES AND THEIR ANTIFOULING BEHAVIOUR DURING ULTRAFILTRATION

In this chapter the synthesized PVDF/TiO_2 nanocomposite via phase inversion route were characterized by permeation tests using Bovine Serum Albumin (BSA) as a model foulant. The BSA filtration experiments have revealed that membrane with 2 wt% of TiO_2 (PM3) exhibits excellent permeation flux, high rejection ratio, and shows good antifouling performance. The adsorption capacity of bovine serum albumin on the membrane surface decreased from 2.85 to 2.15 mg cm^{-2} as the TiO_2 loading increased from 0 to 3 wt% with respect to polymer. Fouling has been found due to cake formation in Ultrafiltration and can be explained by the Hermia's fouling model suggesting that the solutes are not deposited into the pores which interpret that the fouling process is physically reversible.

5.1 INTRODUCTION

Due to non-toxic nature, reasonably high chemical resistance, and relatively low cost, polyvinylidene fluoride (PVDF) is one of the widely used polymers for making membranes for ultrafiltration (UF). However, high hydrophobicity restricts its application and fouling reduces its performance. Fouling of MF and UF membranes due to proteins has been ascribed to adsorption and deposition of proteins on the surface of membranes and within their pores (Marshall et al., 1993). Membrane fouling of UF membranes strongly affects the economic and technological viability of the separation process (Salahi et al., 2010). The fouling is normally classified as reversible fouling which can be easily reversed by physical methods and irreversible fouling which requires special pre-treatment techniques for its elimination (Bhattacharya et al., 2001).Reversible fouling can be eliminated by physical